



## Influence of Thermal Oxidation on the Creep Behavior of Ti-6Al-4V Alloy

Gisele F. C. Almeida<sup>a\*</sup> , Alexandra A. Arbex<sup>a</sup>, Hamon V. S. Oliveira<sup>a</sup>, Nilton I. Domingues<sup>a</sup>,  
Jan Vatauvuk<sup>a</sup>, Danieli A.P. Reis<sup>b</sup> , Marcos Massi<sup>a</sup>, Antônio A. Couto<sup>a,c</sup>

<sup>a</sup>Universidade Presbiteriana Mackenzie, Escola de Engenharia, 01302-907, São Paulo, SP, Brasil.

<sup>b</sup>Universidade Federal de São Paulo, Departamento de Ciência e Tecnologia, 12231-280, São José dos Campos, SP, Brasil.

<sup>c</sup>Instituto de Pesquisas Energéticas e Nucleares, Centro de Ciência e Tecnologia de Materiais, 05508-000, São Paulo, SP, Brasil.

Received: December 05, 2022; Revised: May 17, 2023; Accepted: June 27, 2023

The formation of a stable and adherent oxide layer on the Ti-6Al-4V alloy can improve the mechanical and corrosion resistance of this material. This work studied the creep behavior of Ti-6Al-4V alloy after two different thermal oxidation conditions: at 650 °C for 12 h and at 800 °C for 2 h. In the XRD analysis of the oxidized samples, it was possible to observe the formation of rutile (TiO<sub>2</sub>) and a displacement of the peaks of  $\alpha$  and  $\beta$  phases caused by the dissolution of oxygen. In the creep test at 550 °C, the material oxidized at 800 °C for 2 h showed a greater creep life at 125 MPa, the crack took longer to brake probably due to the greater thickness of the layer. At 550°C and 187.5 MPa the material oxidized at 650 °C for 12h has a better creep life, probably due to the layer more adhered.

**Keywords:** *Thermal oxidation, creep, Ti-6Al-4V alloy.*

### 1. Introduction

Titanium and its alloys are widely used as structural components due to their high mechanical strength, low specific mass, and good corrosion resistance. The Ti-6Al-4V alloy is one of the most important, combining workability and excellent mechanical properties<sup>1</sup>. For this reason, it has been widely used in the aeronautical and aerospace industries, particularly for applications that require mechanical resistance at high temperatures<sup>2</sup>. Due to the high affinity of titanium and its alloys with oxygen, when exposed to an oxygen atmosphere at high temperatures, there is the formation of an oxide layer consisting essentially of rutile (TiO<sub>2</sub>) on its surface and an oxygen diffusion zone, between the oxide layer and the substrate<sup>3</sup>. When exposed to temperatures above 600 °C, the oxide layer becomes thicker and more defective, causing oxygen to penetrate the substrate, leading to material loss and diffusion zone expansion with the formation of hard and brittle layers<sup>4</sup>. In such cases, to generate a titanium oxide barrier layer, a heat treatment is performed using a furnace in the air atmosphere. Thermal oxidation treatments aimed at obtaining ceramic coatings in situ, mainly based on rutile, can offer thick films of highly crystalline oxide, which are accompanied by the dissolution of oxygen underneath them<sup>5</sup>.

According to Dalili et al.<sup>6</sup>, different ranges of treatment time and temperature have been studied in the thermal oxidation treatment of titanium alloys. They mention that higher temperatures with prolonged times result in detachment of the oxide layer and lower temperatures with shorter times result in thinner oxide layers and

insufficiently workable for an improvement in their tribological properties.

Other investigations have been carried out by these authors with the aim of a better understanding of thermal oxidation process in titanium alloys<sup>7-10</sup>. In their work, Severino et al.<sup>8</sup> studied the hot tensile behavior of Ti-6Al-4V alloy after thermal oxidation at 800 °C at different times. Therefore, the present work studied the effects of thermal oxidation and its influence on the mechanical properties of Ti-6Al-4V alloy creep. The results were compared to understand the effects caused by thermal oxidation in the material, as well as the temperature and difference between the stresses exerted in the creep tests. Others works related with creep and oxidation were performed previously by Reis, et al.<sup>11</sup> and Barboza et al.<sup>12,13</sup>. These works considered the oxidation caused during the creep test at high temperatures. However, in this paper, the oxidation was carried out previously with the objective of creating a thermal barrier for future oxidations. The idea arose due to a significant increase in toughness in hot tensile tests of Ti-6Al-4V found in Severino et al.<sup>8</sup> work.

### 2. Materials and Methods

To carry out the present work, Ti-6Al-4V alloy was used in the form of cylindrical bars of 12 mm in diameter. In the condition as received, the bar is mechanically formed, annealed at 800 °C for 2 h and cooled in air. Cylindrical samples of Ti-6Al-4V alloy bar with 2 mm thickness were cut in an Isomet cutter. The samples were prepared by sanding with SiC-based sandpaper in the sequence of 120, 240, 320, 400, 600 and 1200 mesh and polishing with a

\*e-mail: [gisele\\_fab@hotmail.com](mailto:gisele_fab@hotmail.com)

colloidal silica solution. A Kroll solution (5 mL of  $\text{HNO}_3$ , 3 mL of HF and 100 mL of distilled water) is used to etch the specimens. The samples thermal oxidation was carried out in a muffle furnace with temperature control by means of a k-type thermocouple, under two conditions: 650 °C for 12 h (OX650) and 800 °C for 2 h (OX800), both in ambient atmosphere.

An Olympus BX40 optical microscope coupled to a digitalization and image analysis system was used to observe the microstructure, oxide layer and fracture of the creep specimen. A Philips scanning electron microscope coupled with a chemical analysis system using Energy Dispersive Spectroscopy (EDS) was used for the observation and chemical analysis of the layer and observation of the fracture surface of the specimens tested under creep. The analysis of the present phases in Ti-6Al-4V alloy cylindrical samples surface with and without thermal oxidation was performed by X-ray diffractometry using a Rigaku model Multiflex diffractometer and Cu-K $\alpha$  radiation. The specimens were scanned at 2 $\theta$  angles between 20° and 80° with a step increment of 0.02°. The Joint Committee on Powder Diffraction Standards (JCPDS) powder index files were used to identify the XRD results.

The specimens for creep tests were made according to the specifications, gripping systems and extensometers available, according to the ASTM E139-11 standard<sup>14</sup>. The specimens were subjected to thermal oxidation under the same conditions as the cylindrical samples: 650 °C for 12 h and 800 °C for 2 h. Creep tests were performed on a ZwickRoell Kappa 10DS testing machine under the following conditions:

- Specimens without oxidation and oxidized at 800 °C for 2h:
  - 500 °C – Constant load for initial stress of 250 MPa.
  - 550 °C – Constant load for initial stress of 125, 187.5, 250 e 319 MPa.
  - 600 °C – Constant load for initial stress of 250 MPa.
- Specimens oxidized at 650 °C for 12 h:
  - 550 °C – Constant load for initial stress of 125 and 250 MPa.

Due to the number of specimens and the long duration of the creep test, only one test of each condition was performed.

### 3. Results e Discussion

#### 3.1. Microstructural and oxidized layer characterization

Figure 1 shows the oxidized material and the layers formed under the 2 conditions, oxidized for 12 h at 650 °C and oxidized for 2 h at 800 °C. It can be observed in Figure 1 that the microstructure present in the oxidized samples of Ti-6Al-4V alloy is composed of a primary  $\alpha$  (the lightest color phase) and  $\alpha+\beta$  (the darkest color phase), there are no changes in the microstructure after the heat treatments. In the Ti-6Al-4V alloy samples oxidized at 650 °C by at 12 h, the oxide layer presented a thickness between 2.15  $\mu\text{m}$  and 4.07  $\mu\text{m}$  and became more adhered to its surface. In the samples oxidized at 800 °C for 2 h, the oxide layer presented a thickness between 8.68  $\mu\text{m}$  and 11.51  $\mu\text{m}$  and the oxide layer are not adhered to its entire surface, having a more brittle characteristic. According to Kumar et al.<sup>5</sup> the large difference in the coefficient of thermal expansion between titanium oxide and Ti-6Al-4V alloy is responsible for the fragmentation of the substrate oxide layer. Figure 2 illustrates the oxygen diffusion zone of Ti-6Al-4V alloy oxidized at 650 °C for 12 h and at 800 °C for 2 h. Severino et al.<sup>8</sup> found measurements of approximately 15  $\mu\text{m}$  for this same condition and the oxide layer was also non-adherent. Several works are found in the literature where the Ti-6Al-4V alloy is oxidized at different temperatures, between 500 and 800 °C.

Dong and Bell<sup>15</sup> studied the oxidized Ti-6Al-4V alloy to verify its wear behavior. They conducted the oxidation in an atmosphere containing about 80% oxygen and 20% nitrogen at 600 °C for 65 h. The microstructure of the oxidized material was composed of a thin rutile oxide layer of approximately 2  $\mu\text{m}$ , followed by an oxygen diffusion zone (ODZ) of approximately 20  $\mu\text{m}$ . The diffusion zone is characterized by a lighter shade of gray just below the oxide layer. The diffusion zone of the oxidized sample at 650 °C for 12 h was almost imperceptible and the oxide layer was well adhered. As for the oxidation at 800 °C for 2 h, the diffusion zone became thicker, and the oxide layer was not adhered.

Severino et al.<sup>8</sup> studied the hot tensile behavior of Ti-6Al-4V alloy oxidized at 800 °C for 0.5, 1, 5, 10, 20 and 40 h. The results showed a significant increase in toughness, mainly in the oxidized condition for 2 h. Güleriyüz and

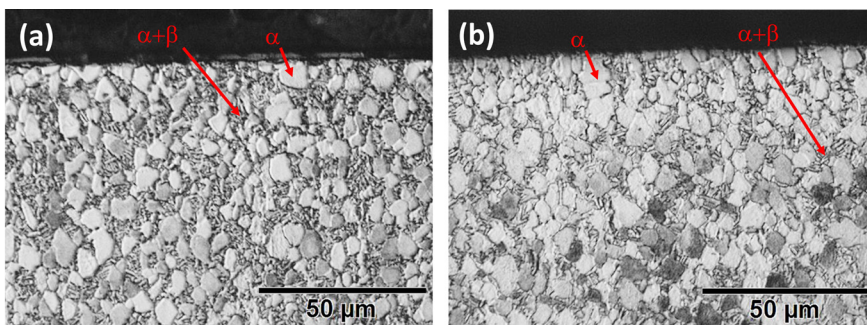


**Figure 1.** Optical microscopy of the microstructure of oxidized samples (a) at 650 °C for 12 h and (b) at 800 °C for 2 h. The arrows indicate the present phases.

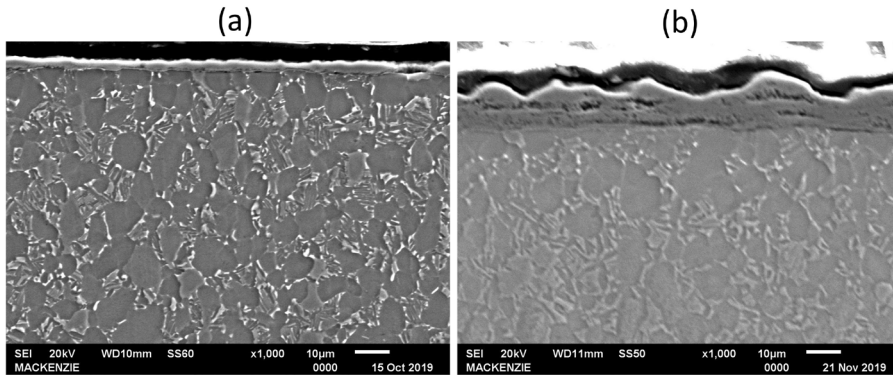


**Figure 2.** Scanning electron micrographs of oxidized samples (a) at 650 °C for 12 h and (b) at 800 °C for 2 h.

Cimenoglu<sup>16</sup> oxidized Ti-6Al-4V alloy to study corrosion wear performance. Oxidation conditions were 600 °C and 650 °C between 12 and 60 h under not controlled atmospheric conditions. The results showed an oxygen diffusion zone below the oxide layer. At low temperature, thin oxide films were observed, increasing temperature and oxidation time promoted the formation of thick oxide layers and deeper penetration of oxygen into the metal. In another work<sup>17</sup>, they examined the effect of thermal oxidation on the dry sliding wear resistance of Ti-6Al-4V alloy. Oxidation at 600 °C for 60 h introduced hard surface layers composed of TiO<sub>2</sub> and an oxygen diffusion zone beneath it. Surface hardness increased by approximately 3 times after oxidation.

Kumar et al.<sup>18</sup> studied the thermal oxidation of Ti-6Al-4V alloy at 500, 650 and 800 °C for 8, 16, 24 and 48 h in air. The morphological characteristics of the surface revealed that the formed oxide film is adherent to the substrate at 500 and 650 °C, regardless of the oxidation time, while it fragments when the alloy is oxidized at 800 °C. The large volume ratio of rutile to Ti and the large difference in coefficient of thermal expansion between rutile and titanium are considered responsible for the fragmentation of the oxide layer. It was concluded that, at lower temperatures, the oxide layer formed is thinner and adheres better. The increase in treatment time allows for an increase in the size of the oxide particles and filling of the entire surface. However, an excessive increase can result in more agglomeration and more porosity of the oxide layer, making it less adherent.

Figure 3 shows the X-ray diffractogram of the samples under the 3 conditions: without oxidation, oxidized at 650 °C for 12 h and oxidized at 800 °C for 2 h. In the sample without oxidation, only the peaks referring to the  $\alpha$  and  $\beta$  phases are observed. In fact, only the peak (110) of  $\beta$  phase can be observed. In oxidized samples, in addition to the  $\alpha$  phase, rutile (TiO<sub>2</sub>) can be observed. The  $\beta$ -phase peaks cannot be observed in the oxidized samples. Zhang et al.<sup>19</sup> justify the absence of  $\beta$  phase after oxidation due to oxygen being a stabilizer of  $\alpha$  phase. In this work, as in others cited, only rutile was detected by X-ray diffraction. Other oxides were not detected by X-ray diffraction. Note a shift in the position of  $\alpha$ -phase peaks in the oxidized samples. This fact is due to the diffraction of the layer with diffused oxygen just below the titanium oxide. Oxygen in the crystalline lattice of titanium causes a change in the lattice parameters of  $\alpha$  phase and consequently in the angles of the diffracted planes.

The chemical composition of the surface layer was verified by Energy Dispersive Spectrometry (EDS) in the Scanning Electron Microscope. Figures 4 and 5 show the composition of the oxide layer under the 2 thermal oxidation conditions. It is possible to observe that the layer is composed of titanium and oxygen in the middle region and aluminum and oxygen in the outermost range of the layer. Casadebaigt et al.<sup>20</sup> describe that the oxide layer formed at 500–600 °C of Ti-6Al-4V alloy fabricated by Laser and Electron Beam Melting is mainly composed of rutile (TiO<sub>2</sub>) with presence of alumina (Al<sub>2</sub>O<sub>3</sub>). In Figures 4 and 5, as well as in the study by Zhang et al.<sup>19</sup>, it is possible to observe, analyzing the external oxidized layer, that an aluminum-poor region appears near the oxide/ODZ interface, indicating that the external diffusion of Al atoms occurs to form alumina near the gas/oxide interface. In addition, there is a higher aluminum content and a lower titanium content in the outer part of the oxide. Therefore, alumina grows outwards while rutile grows mostly inwards.

According to Zhang et al.<sup>19</sup>, the Ti-6Al-4V alloy oxidation mechanism can be divided into four stages. In the first step, the formation of thin rutile nuclei preferentially occurs, since the activation energy of rutile is much lower than that of alumina. With increasing oxidation time, rutile cores will gradually cover the surface of the alloy. In the second stage, rutile continues to form at the gas/oxide and oxide/alloy interfaces through external diffusion of titanium and internal diffusion of oxygen. Addition of vanadium can effectively reduce aluminum activity. Therefore, the formation of alumina at the oxide/alloy interface is avoided. In the third stage, nodular alumina begins to appear at the gas/oxide interface. The existence of vanadium in the alloy reduces the solubility of the aluminum and causes it to diffuse out. If activated titanium atoms are insufficient at the oxide/alloy interface, aluminum atoms will be promoted to diffuse out and react with oxygen. In this case, nodular alumina becomes the preferred oxidation product at the gas/oxide interface. In the fourth step the oxygen diffusivity through the oxide layer and the subsequent scale growth rate are reduced due to the blocking effect of alumina. Meanwhile, a new oxide grows in the gaps between adjacent large nodular particles, leading to the formation of a mixed oxide layer composed of rutile and alumina.

Du et al.<sup>21</sup> observed that nodular nuclei of Al<sub>2</sub>O<sub>3</sub> developed on the surface of the sample in the early stages of oxidation



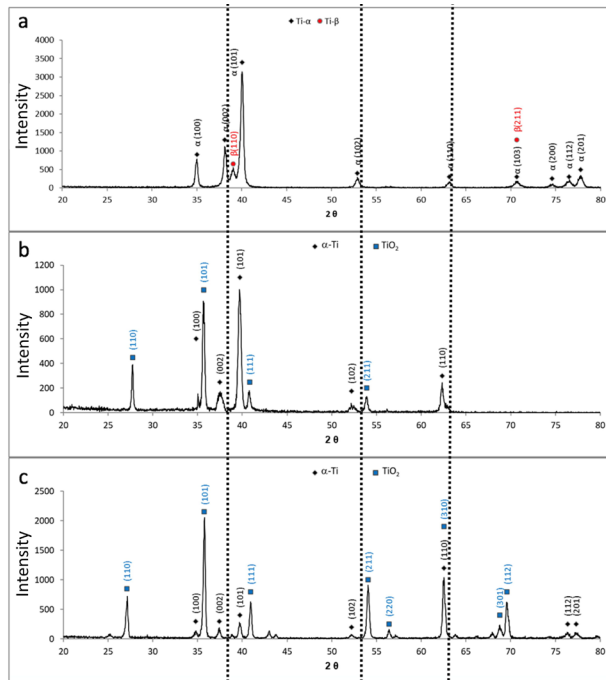


**Figure 3.** X-ray diffractogram of Ti-6Al-4V alloy (a) without thermal oxidation, (b) oxidized at 650 °C for 12 h, and (c) oxidized at 800 °C for 2 h. The vertical dotted lines help to see the peak dislocation.

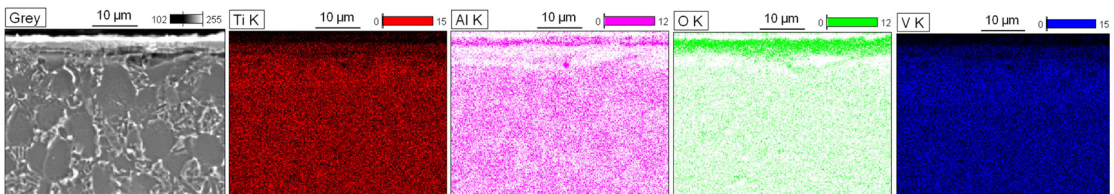


**Figure 4.** Composition of the layer formed in oxidation at 650 °C for 12 h.

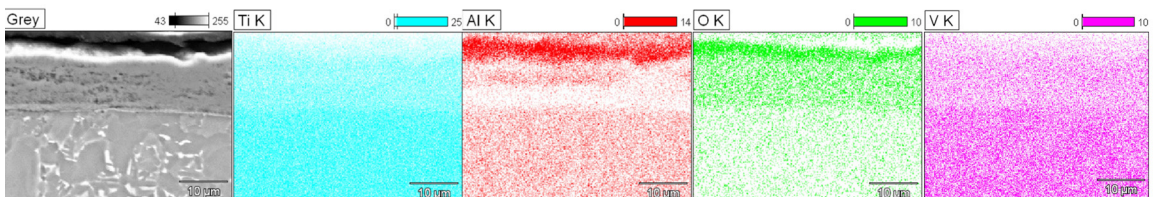


**Figure 5.** Composition of the layer formed in the oxidation at 800 °C for 2 h.

along with a thin layer of  $\text{TiO}_2$ .  $\text{Al}_2\text{O}_3$  nuclei grew laterally with increasing oxidation time and completely covered  $\text{TiO}_2$ . Their results also showed an  $\alpha$ - $\text{Al}_2\text{O}_3$  layer at the outer interface of the oxide layers for all oxidized samples and that a titanium layer formed at the oxide/substrate layer interface, while an  $\text{Al}_2\text{O}_3$  layer formed at the gas/oxide interface. external. As the oxidation times were up to 100 h, it was possible to observe the  $\text{Al}_2\text{O}_3$  layer and the  $\text{TiO}_2$  layer growing alternately, producing multiple layers.

### 3.2. Creep tests results

Table 1 presents the results of the creep test at temperatures of 500 to 600 °C and stresses of 125 to 319 MPa of Ti-6Al-4V alloy, in the specimens without and with thermal oxidation. This table summarizes the main experimental parameters, the values of the primary creep time ( $t_p$ ), the secondary creep rate ( $\dot{\epsilon}_s$ ), the final creep time ( $t_f$ ) and the final strain ( $\epsilon_f$ ). According to Table 1, the tests carried out at 550 °C and 125 MPa indicated that the materials oxidized

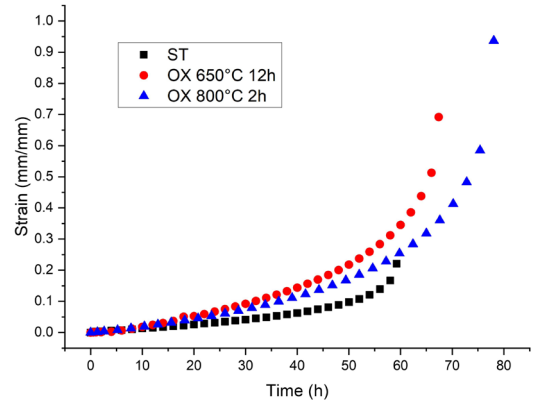
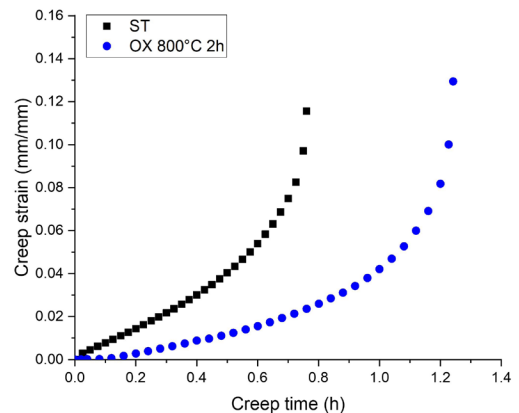
**Table 1.** Parameters and results of creep tests.

Temperature (°C)	Stress (MPa)	Condition	$t_p$ (h)	$\dot{\epsilon}_s$ (1/h)	$t_f$ (h)	$\epsilon_f$ (mm/mm)	RA (%)
500	250	OX800	1.00	0.00094	58.56	0.16	61.9
		ST	1.19	0.00044	67.39	0.06	68.1
		OX650	6.00	0.00404	67.39	0.69	86.7
	125	OX800	1.30	0.00272	78.05	0.94	90.5
		ST	1.00	0.00140	59.30	0.22	71.0
		OX650	1.00	0.01030	13.81	0.36	76.2
550	187.5	OX800	0.20	0.00320	5.88	0.06	76.9
		ST	0.45	0.00350	4.56	0.02	75.8
		OX650	0.13	0.05173	3.60	0.40	56.2
	250	OX800	0.24	0.05253	3.58	0.40	57.7
		ST	0.44	0.03280	0.69	0.05	65.9
		OX800	0.08	0.03342	1.24	0.13	56.4
319	ST	0.09	0.07962	0.76	0.12	57.0	
	OX800	0.04	0.12844	0.49	0.13	87.1	
600	250	ST	0.06	0.38395	0.59	0.76	75.1

at 650 °C/12 h (OX650) and at 850 °C/2 h (OX800) present a higher reduction in area and creep life when compared to the material not oxidized (ST). In the tests carried out at 550 °C and 187.5 MPa, the oxidized material also presented a longer creep life, in this case the material oxidized at 650 °C for 12h has a better creep life, probably due to the layer more adhered. In the tests carried out at 500 °C and 250 MPa, the oxidized material presented a lower creep life. The material oxidized and subjected to creep at 600 °C and 250 MPa presented a shorter creep life. This temperature was too high at the stress used in the tests, with very low creep life, and close between the oxidized and non-oxidized alloy, not allowing a consolidated conclusion of the effect of thermal oxidation. The tests carried out at 550 °C and 319 MPa showed higher creep life for the oxidized material in relation to the non-oxidized material.

At 550 °C and at all stresses used in the creep tests, the oxidized material showed a longer creep life under both oxidation conditions (OX650 and OX800) compared to the material not subjected to thermal oxidation (ST). In the creep test at 550 °C and 125 MPa, the material oxidized at 800 °C/2 h showed a longer creep life than the one oxidized at 650 °C/12 h and without oxidation, also showing the highest reduction in area. Comparing the secondary creep rates with the different treatment conditions, there was no significant reduction in the creep speed in any of the conditions, and the increase in creep life in some conditions of the oxidized material may be related to the alloy surface hardening, as observed in previous work<sup>22</sup>.

Figure 6 shows the results of tests carried out at 550 °C with 125 MPa on the oxidized material and as without treatment. In this condition, a longer time to fracture and a lower secondary creep rate are observed for the material oxidized at 800 °C for 2 h compared to the material oxidized at 650 °C for 12 h, the crack took longer to brake probably due to the greater thickness of the layer. Figure 7 shows the results of the tests carried out at 550 °C with 319 MPa on the material without treatment and oxidized at 800 °C for 2 h. In this case, as it is a more severe temperature and stress condition, a significant improvement in the creep resistance of the oxidized material can be noted. The increased creep

**Figure 6.** Creep curves for ST, OX650, and OX800 conditions at 550 °C and 125 MPa stress.**Figure 7.** Creep curves for non-oxidized and oxidized conditions at 800 °C for 2 h at a temperature of 550 °C and a stress of 319 MPa.

life under some conditions of the oxidized material may be related to the alloy surface hardening<sup>22</sup>. Which may be associated with the previous formation of a stable oxide.

The dependence of the stress values and the secondary creep rate can be related by the logarithmic function described in the Power-Law creep Equation 1:

$$\dot{\epsilon}_s = B\sigma^n \quad (1)$$

Where  $B$  is a constant dependent on the material microstructure,  $n$  is the stress exponent and  $\sigma$  is the applied stress. The dependence of temperature on creep rate can be represented by the Arrhenius equation shown in Equation 2. And the values of activation energy ( $Q_c$ ) can be calculated by Arrhenius Law:

$$\dot{\epsilon}_s = B_0\sigma^n \exp(-Q_c / RT) \quad (2)$$

Where  $B_0$  is a constant dependent on the material microstructure,  $R$  is the universal gas constant and  $T$  is the applied absolute temperature.

The value for parameter “ $n$ ” for the material oxidized at 800 °C for 2 h and the material without oxidation were respectively 3.29 and 4.06 and  $B_0$  were  $3,36 \times 10^4$  and  $4,59 \times 10^4$ . The value for the “ $Q_c$ ” parameter was 279 kJ/mol for the material oxidized at 800 °C for 2 h and 382 kJ/mol for the one without oxidation. These values found are within the range found in the literature and which indicate a predominance of creep behavior influenced by climb of dislocations. Barbosa et al.<sup>12</sup> found values of 4.12 for  $n$  and 319 kJ/mol for  $Q_c$ , for the Ti-6Al-4V alloy with equiaxed microstructure and tests performed at 500 °C. Brigunte et al.<sup>23</sup> found values of 3.59 for  $n$  and 266 kJ/mol for  $Q_c$  for the same material tested at 600 °C.

The  $M$  parameter corresponds to a measure of the influence of the secondary creep rate ( $\dot{\epsilon}_s$ ) on the creep rupture time ( $t_f$ ) and is the well-known Monkman-Grant relationship, where  $M$  and  $C$  are the constants. This relation is described in Equation 3:

$$t_f (\dot{\epsilon}_s)^M = C \quad (3)$$

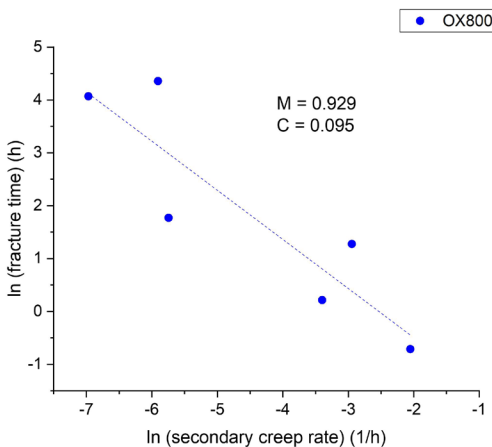


**Figure 8.** Dependency of the creep rupture time with the steady-state creep rate of the material oxidized at 800 °C for 2 h.

Figure 8 shows the relationship between creep rupture time and steady-state creep rate for all test conditions of 500, 550 and 600 °C and stresses of 125, 187.5, 250 and 319 MPa, material oxidized at 800 °C for 2 h. The proportionality between  $\dot{\epsilon}_s$  and  $t_f$  obtained by linear regression techniques was  $M = 0.929$  and  $C = 0.095$ . In general, values of  $M$  approximately equal to one are found for several materials, indicating a proportionality between the rupture time and the deformation rate in the secondary stage, as proposed by Evans et al.<sup>24</sup>.

Figure 9 shows the dependence of fracture time on stress. Using linear regression techniques, the results can be described according to Equation 4 of the creep Power law:

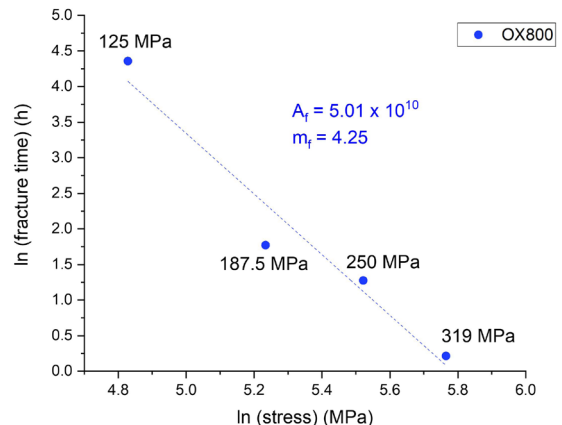
$$t_f = A_f \sigma^{-m_f} \quad (4)$$

where the parameters  $A_f$  and  $m_f$  are normally determined by creep tests under constant load and depend on the temperature of the material, composition, and microstructure. For the oxidized condition at 800 °C for 2 h, the values obtained were  $5.01 \times 10^{10}$  and 4.25, respectively.

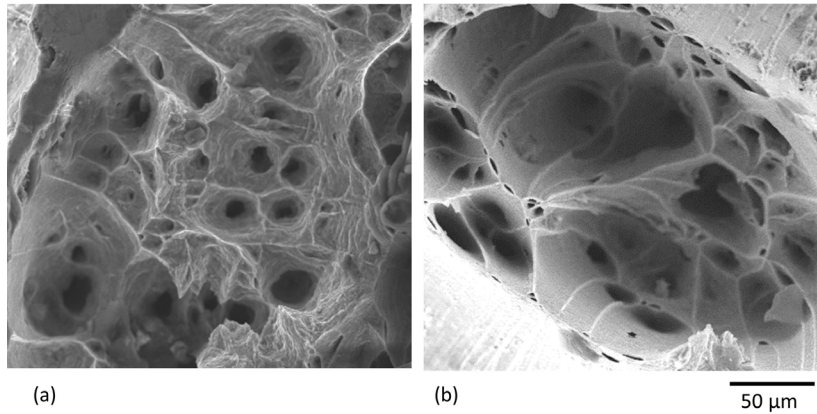
### 3.3. Fractographic analysis

Figure 10 show the fracture surfaces of the specimens after the creep test at 550 °C and 125 MPa under oxidized and not oxidized conditions. In the fracture region, a ductile fracture is observed with the presence of microcavities (dimples) and an extensive deformed region with significant material stricture. Figure 11 shows side views of the fractured specimens after creep tests at 550 °C and 125 MPa. The characteristics observed in the fractures in the creep test condition at 550 °C and 125 MPa were like those observed in test conditions with temperatures and stresses higher than these. It is possible to observe that the oxidized layer formed in the 3 tested conditions: without thermal oxidation and oxidized at 650 °C for 12 h and 800 °C for 2 h. In the condition without oxidation, a smaller layer is formed for the time that the specimen was exposed to a temperature of 550 °C during the test. These fragmented scales were also observed by Jamesh et al.<sup>25</sup>.

In Figure 12, optical micrographs of specimens oxidized at 800 °C for 2 h and evaluated in creep at 550 °C



**Figure 9.** Dependency of creep rupture time with stress at 550 °C for material oxidized at 800 °C for 2 h.



**Figure 10.** Fracture surfaces of specimens after creep testing at 550 °C and 125 MPa (a) without oxidation, (b) oxidized at 650 °C for 12 h, and (c) oxidized at 800 °C for 2 h.

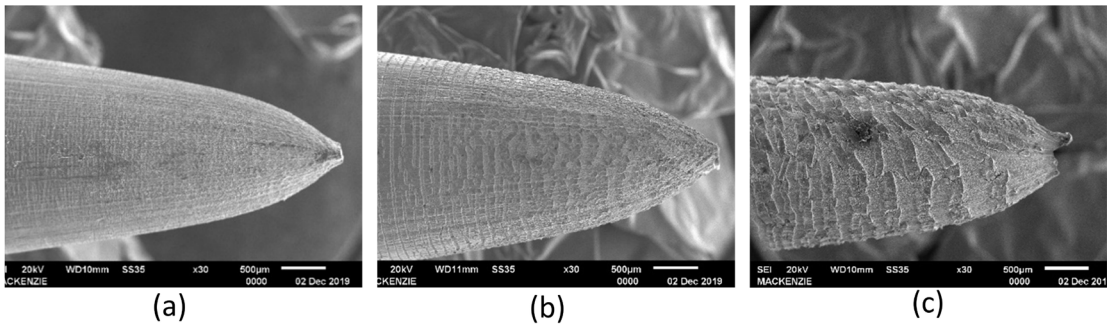


**Figure 11.** Surfaces of specimens tested in creep at 550 °C and 125 MPa (a) without oxidation, (b) oxidized at 650 °C for 12 h, and (c) oxidized at 800 °C for 2 h.

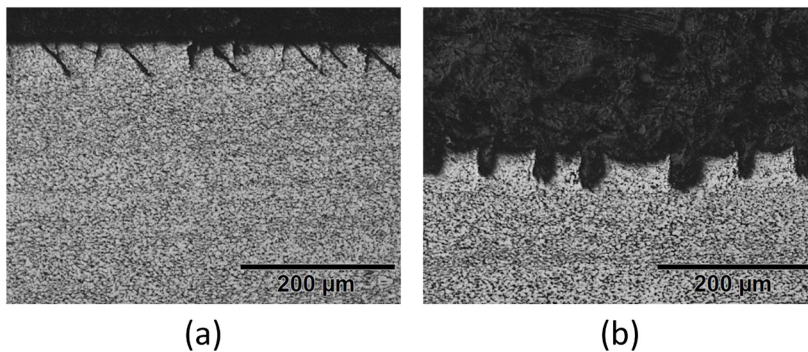


**Figure 12.** Longitudinal sections of specimens oxidized at 800 °C for 2 h and tested under creep at a temperature of 550 °C and stress of (a) 125 MPa, and (b) 319 MPa.

and tensions of 125 and 319 MPa in longitudinal section are shown. Both oxidized layers show rupture, but with differences between them. In the creep test at lower stress (125 MPa) the cracks are narrower, as seen in Figure 12a. In the specimen tested at higher tension (319 MPa) there is already a marked separation in the cracks, forming a kind of dent along the entire length of the specimen, as shown in Figure 12b. Figure 13a shows in detail the layer thermally

oxidized at 800 °C for 2 h and flow tested at 550 °C and 125 MPa. In this Figure, the fragiley broken oxide layer is evident, with the presence of cleavage. Figure 13b shows the fracture of the oxidized material at 650 °C for 12 h and tested at 550 °C and 250 MPa. Note in this fractography distinct characteristics in the various regions of the fractured specimen. On the surface of the specimen, the presence of the oxidized layer is fragiley fractured with the presence of



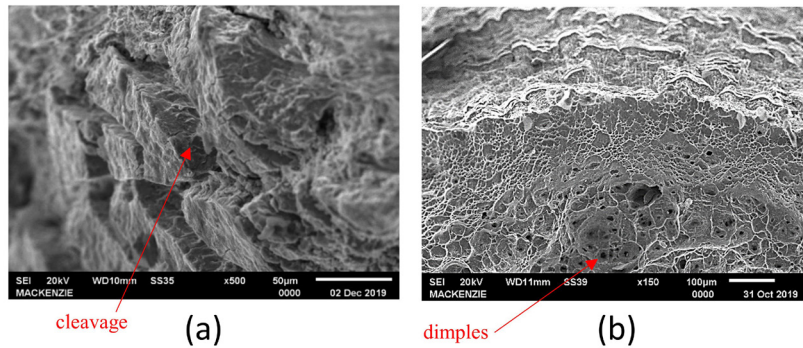


**Figure 13.** Images of the (a) fracture surface and (b) internal region of the oxidized specimen at 650 °C for 12 h and tested in creep at 550 °C and 250 MPa. The red arrows indicate the region of cleavage and dimples.

cleavage. In the central region of the specimen section, the presence of microcavities (dimples) is observed, characteristic of ductile fracture. Between the oxidized region of the surface and the central section of the specimen, a transition region can be observed, with the presence of microcavities, but shallower than those in the central region.

### 3.4. Final considerations

In general, the oxide layer formed on the surface of the Ti-6Al-4V alloy due to thermal oxidation showed an increase in the final creep time. The oxide layer has retarded the crack nucleation. After the cracks nucleate in the fragile oxide layer of the specimens submitted to thermal oxidation, the Ti-6Al-4V alloy is led to fracture due to the deformation and propagation of these cracks. The thicker oxidized layer at the oxidation temperature of 800 °C appears to have a beneficial effect on creep life under almost all test conditions. In creep tests at higher stresses and temperatures, it is not possible to define a behavior trend between thermally oxidized and untreated specimens due to the short time for fracture under these conditions. In creep tests at the lowest stress (125 MPa) and intermediate temperature (550 °C) the improvement in creep life due to thermal oxidation is clear, especially for specimens oxidized at 800 °C/2 h.

## 4. Conclusions

The study on the influence of thermal oxidation on the creep behavior of Ti-6Al-4V alloy led to the conclusion that:

- In the Ti-6Al-4V alloy oxidized at 650 °C for 12 h, the layer had a thickness between 2.15 and 4.07 µm and was adhered to the entire surface of the sample. The diffusion zone of the samples was almost imperceptible, and the oxide layer was well adhered. In the material oxidized at 800 °C for 2h, the layer presented a thickness between 8.68 to 11.51 µm and the oxide layer was not adhered to the entire surface, having a more brittle characteristic. The diffusion zone became thick, and the oxide layer was not adhered.
- It is possible to observe the presence of a mixed oxide layer composed of rutile and alumina, with an aluminum poor region near the oxide-oxygen diffusion zone interface, indicating that the external

diffusion of Al atoms occurs to form alumina near the gas/oxide interface.

- In the X-ray diffraction analysis, only rutile was detected, in addition to the  $\alpha$  and  $\beta$  phases of Ti. A displacement of the  $\alpha$  and  $\beta$  phases peaks can be observed in the oxidized sample, caused by the dissolution of oxygen in the subsurface zone.
- The values of “n” of 3.29 and 4.06 and Qc of 279 kJ/mol and 382 kJ/mol for the material oxidized at 800 °C for 2 h and for the one without oxidation respectively indicate a predominance of creep behavior influenced by climb of dislocations.
- The Monkman–Grant parameter (M) for all test conditions of 500, 550 and 600 °C and stresses of 125, 187.5, 250 and 319 MPa of material oxidized at 800 °C for 2 h was 0.929, indicating a proportionality between the rupture time and the deformation rate in the secondary stage.
- In the creep test at 550 °C, the material oxidized at 800 °C for 2 h showed a lower creep rate at stresses 125 and 187.5 MPa. In the creep tests at 550 °C and 319 MPa and 600 °C and 250 MPa, the material oxidized at 800 °C for 2 h also showed a lower rate in relation to the material without oxidation.
- In the creep test at lower stress, the cracks are narrower, while in the test at higher tension there is already a marked separation in the cracks, forming a kind of tooth along the entire length of the specimen.
- On the surface of the specimen, the presence of an oxidized and brittle fractured layer with the presence of cleavage can be noted. In the central region of the section of the specimen, the presence of microcavities, characteristic of ductile fracture, can be observed. Between the oxidized region of the surface and the central section of the specimen, there is a transition region, with the presence of shallower microcavities than those in the central region.

## 5. Acknowledgments

Funding: This work was supported by Coordination of Superior Level Staff Improvement (CAPES), Brazil - Finance Code 001 [grant number 88887.583658/2020-00].



## 6. References

- Gülyeryüz H, Cimenoglu H. Surface modification of a Ti-6Al-4V alloy by thermal oxidation. *Surf Coat Tech.* 2005;192(2-3):164-70.
- Briguinte LANS, Oñoro J, Briguinte FP, Resende FA, Reis JL, Reis DAP, et al. The influence of laser nitriding on creep behavior of Ti-4Al-4V alloy with widmanstätten microstructure. *Metals.* 2019;9(2):236. <https://doi.org/10.3390/met9020236>.
- Uwanyuze RS, Alpay SP, Schafföner S, Sahoo S. A first principles analysis of oxidation in titanium alloys with aluminum and vanadium. *Surf Sci.* 2022;719:122026.
- Batory D, Szymanski W, Panjan M, Zabeida O, Klemberg-Sapieha JE. Plasma nitriding of Ti6Al4V alloy for improved water erosion resistance. *Wear.* 2017
- Kumar S, Narayanan TSNS, Raman SGS, Seshadri SK. Thermal oxidation of CP Ti: an electrochemical and structural characterization. *Mater Charact.* 2010;61(6):589-97.
- Dalili N, Edrisy A, Farokhzadeh K, Li J, Lo J, Riahi AR. Improving the wear resistance of Ti-6Al-4V/TiC composites through thermal oxidation (TO). *Wear.* 2010;269(7-8):590-601.
- Reis DAP, Piorino F No, Barboza MJR, Nono MCA, Silva CRM. Influence of the oxidation in creep of Ti-6Al-4V alloy. *Acta Microsc.* 2003;12(Suppl):219-20.
- Severino BP, Couto AA, Reis DAP, Aguiar CL, Castagnet M, Moura Neto C. Study of high temperature mechanical behavior of the thermally oxidized Ti-6Al-4V alloy. *Materialwiss Werkstofftech.* 2014;45(4):269-80.
- Champin B, Graff L, Armand M, Béranger G, Coddet C. Oxydation des alliages de titane au voisinage des températures d'utilisation dans les turbomoteurs. *J Less Common Met.* 1980;69(1):163-83.
- Gemelli E, Camargo NHA. Oxidation kinetics of commercially pure titanium. *Rev Matéria.* 2007;12(3):525-31.
- Reis DAP, Silva CRM, Nono MCA, Barboza MJR, Piorino F No, Perez EAC. Effect of environment on the creep behavior of the Ti-6Al-4V alloy. *Mater Sci Eng A.* 2005;399(1-2):276-80.
- Barboza MJR, Moura C No, Silva CRM. Creep mechanisms and physical modeling for Ti-6Al-4V. *Mater Sci Eng A.* 2004;369(1-2):201-9.
- Barboza MJR, Perez EAC, Medeiros MM, Reis DAP, Nono MCA, Piorino F No, et al. Creep behavior of Ti-6Al-4V and a comparison with titanium matrix composites. *Mater Sci Eng A.* 2006;428(1-2):319-26.
- ASTM: American Society for Testing and Materials. ASTM E139-11 Standard Test Methods for Conducting Creep, Creep Rupture, and Stress Rupture Tests of Metallic Materials. West Conshohocken: ASTM; 2011. p. 11.
- Dong H, Bell T. Enhanced wear resistance of titanium surfaces by a new thermal oxidation treatment. *Wear.* 2000;238(2):131-7.
- Gülyeryüz H, Cimenoglu H. Effect of thermal oxidation on corrosion and corrosion-wear behaviour of a Ti-6Al-4V alloy. *Biomaterials.* 2004;25(16):3325-33.
- Guleryuz H, Cimenoglu H. Oxidation of Ti-6Al-4V alloy. *J Alloys Compd.* 2009;472(1-2):241-6.
- Kumar S, Sankara Narayanan TSN, Raman SGS, Seshadri SK. Thermal oxidation of Ti6Al4V alloy: microstructural and electrochemical characterization. *Mater Chem Phys.* 2010;119(1-2):337-46.
- Zhang Y, Ma GR, Zhang XC, Li S, Tu ST. Thermal oxidation of Ti-6Al-4V alloy and pure titanium under external bending strain: experiment and modelling. *Corros Sci.* 2017;122:61-73.
- Casadebaigt A, Hugues J, Monceau D. High temperature oxidation and embrittlement at 500–600 °C of Ti-6Al-4V alloy fabricated by Laser and Electron Beam Melting. *Corros Sci.* 2020;175:108875.
- Du HL, Datta PK, Lewis DB, Burnell-Gray JS. Air oxidation behaviour of Ti6Al4V alloy between 650 and 850°C. *Corros Sci.* 1994;36(4):631-42.
- Almeida GFC, Couto AA, Reis DAP, Massi M, Silva AS, Lima NB. Estudo da Nitretação por Plasma na Fluência da Liga Ti-6Al-4V. *Tecnol em Metal Mater e Mineração.* 2016;13(4):331-9.
- Briguinte FP, da Silva Briguinte LAN, Reis DAP, da Silva MM. Comparative Study of Creep Resistance of a Ti-6Al-4V Alloy with Metallic and Ceramic Coatings. *Mater Sci Forum.* 2014;802:472-6.
- Evans RW, Wilshire B. Introduction to creep. London, England: The Institute of Materials; 1993.
- James M, Sankara Narayanan TSN, Chu PK. Thermal oxidation of titanium: evaluation of corrosion resistance as a function of cooling rate. *Mater Chem Phys.* 2013;138(2-3):565-72.